Synoptic-Statistical Approach to Regional Downscaling of IPCC Twenty-First-Century Climate Projections: Seasonal Rainfall over the Hawaiian Islands*

OLIVER TIMM

IPRC, SOEST, University of Hawaii at Manoa, Honolulu, Hawaii

HENRY F. DIAZ

CIRES Climate Diagnostics Center, Boulder, Colorado

(Manuscript received 10 September 2008, in final form 25 February 2009)

ABSTRACT

A linear statistical downscaling technique is applied to the projection of the Intergovernmental Panel on Climate Change (IPCC) Fourth Assessment Report (AR4) climate change scenarios onto Hawaiian rainfall for the late twenty-first century. Hawaii's regional rainfall is largely controlled by the strength of the trade winds. During the winter months, disturbances in the westerlies can produce heavy rainfall throughout the islands. A diagnostic analysis of sea level pressure (SLP), near-surface winds, and rainfall measurements at 134 weather observing stations around the islands characterize the correlations between the circulation and rainfall during the nominal wet season (November–April) and dry season (May–October). A comparison of the base climate twentieth-century AR4 model simulations with reanalysis data for the period 1970–2000 is used to define objective selection criterion for the AR4 models. Six out of 21 available models were chosen for the statistical downscaling. These were chosen on the basis of their ability to more realistically simulate the modern large-scale circulation fields in the Hawaiian Islands region.

For the AR4 A1B emission scenario, the six analyzed models show important changes in the wind fields around Hawaii by the late twenty-first century. Two models clearly indicate opposite signs in the anomalies. One model projects 20%–30% rainfall increase over the islands; the other model suggests a rainfall decrease of about 10%–20% during the wet season. It is concluded from the six-model ensemble that the most likely scenario for Hawaii is a 5%–10% reduction of the wet-season precipitation and a 5% increase during the dry season, as a result of changes in the wind field. The authors discuss the sources of uncertainties in the projected rainfall changes and consider future improvements of the statistical downscaling work and implications for dynamical downscaling methods.

1. Introduction

The Intergovernmental Panel for Climate Change (IPCC) Fourth Assessment Report (AR4) leaves no doubt that the increase in atmospheric CO_2 concentration will lead to significant environmental changes in all regions of the globe (Solomon et al. 2007). However, the degree of uncertainty of the projected climate changes increases from global to regional scale. Small-scale topographic features such as the Hawaiian Islands are below the typical horizontal and vertical resolution of the GCMs and cannot be represented. To project the large-scale climate changes onto regional scales, nested regional models or statistical methods have been adopted (von Storch et al. 1993; Wilby and Wigley 1997; Christensen et al. 2007; Schmidli et al. 2007; Wang and Zhang 2008). Here, we will apply statistical downscaling (SD) to the rainfall of the Hawaiian Islands under the assumptions that GCMs best simulate the large-scale atmospheric circulation patterns and that future changes in those principal climate modes would be the most likely to affect the climate of Hawaii.

The Hawaiian Islands are located in the trade wind zone southwest of the subtropical high pressure system of the North Pacific Ocean. As noted above, the small-scale topographic features of the islands are not represented in

* International Pacific Research Center Contribution Number 596 and School of Ocean and Earth Science and Technology Contribution Number 7657.

Corresponding author address: Oliver Timm, 1680 East-West Rd., Honolulu, HI 96822.
E-mail: timm@hawaii.edu

DOI: 10.1175/2009JCLI2833.1

the suite of Solomon et al. (2007) GCMs, and therefore the interaction between the large-scale circulation and high topography of the islands must be considered in order to obtain a regionally consistent estimate of projected rainfall changes over Hawaii.

The climate of Hawaii is characterized by a wet (during the Northern Hemisphere winter half-year) and a dry (summer) season. Four different mechanisms for rainfall production have been identified in previous meteorological studies (Schroeder 1993; Chu et al. 1993). Lyons (1982) found that trade wind–induced rainfall along the windward-facing sides of the mountain chains is the most significant contributor to the statewide rainfall budget. The strong covariance between precipitation on Hawaii and the trade wind circulation that was found in earlier studies suggests that the SD of large-scale circulation patterns onto Hawaiian rainfall stations is feasible, despite the complexity of the physical processes that actually control the formation of precipitation (Woodcock 1975; Ramage and Schroeder 1999; Yang and Chen 2003; Cao et al. 2007). In addition, frontal rain associated with extratropical storms over the North Pacific is observed during the wet season. Cold air troughs dipping far to the south sometimes become detached from the main westerly circulation and develop a cutoff low pressure system known as a kona low. This leads to advection of moist warm air masses from the equatorial Pacific to the islands, and the cool air aloft provides the thermodynamic instability for the development of intense rainfall events. The island topography can locally force extreme rainfall events of 10–12 inches in 24 h. These extreme rainfall events contribute up to more than 50% of the annual rainfall total on the drier leeward sides of the islands (except for the leeward side of the Big Island with the two big volcanoes that reach to ~4100 m in elevation). Therefore, much of the interannual-to-decadal variability is determined by relatively few events (see also Chu and Chen 2005), which will make the task for statistical climate change projections more difficult than in regions with a higher frequency of rainfall events, such as along the windward-facing mountain chains.

The present study aims for a first quantitative assessment of the expected mean seasonal rainfall changes given the projected circulation changes under the A1B emission scenario. Regionalized precipitation change information can serve many purposes. For example, Hawaii's ecosystems are vulnerable to disturbances in the climatological pattern under global warming. Changes in rainfall could impose a severe stress on endemic species (Loope 1995; Loope and Giambelluca 1998). On the stakeholders' side, water resource management plans would need to be revised if Hawaii was expected to experience significant changes in the rainfall under global warming (Oki 2004). We emphasize that the present study is a first attempt to downscale the large-scale circulation changes of the twenty-first century from the AR4 onto individual rainfall stations on the Hawaiian Islands. In section 2, the data and methods are described. Section 3 presents the results from diagnostic studies and the calibration and validation of the statistical transfer model. Further, the evaluation of the various GCMs from the IPCC AR4 are presented and finally the results from the twenty-first-century climate change downscaling are presented. In section 4, a discussion of the associated uncertainties is given. Section 5 will summarize the results and closes with concluding remarks on future improvements for statistical downscaling.

2. Data and methods

SD involves three essential steps: first, the establishment of a statistical relationship between the large-scale predictors and the local predictands; second, an assessment of the predictive skill of the statistical model and third the application of the statistical model (Wilby and Wigley 1997). For the application to the twenty-first-century climate change simulations, the SD method must further include an analysis and selection of the GCM scenario runs, with the goal to select those models that compare best to the observed climate during the twentieth century. The chosen models will provide the predictor information for the third step of the SD.

Daily and monthly rainfall data were obtained from the National Climatic Data Center in Asheville, North Carolina. Originally, stations with less than 10% missing data were used to form monthly mean rainfall values. In this study, the majority of the records are available for the period 1950 to the present. The climatological annual cycle in Hawaiian rainfall has been previously studied (Giambelluca et al. 1986). Most regions in Hawaii experience a pronounced seasonal cycle of precipitation (Fig. 1), with the bulk of the precipitation falling during the months of November through April (the wet season) and less frequent rainfall events during the months May through October (the dry season). Hence, we will develop SD projection scenarios for the dry and wet season. For the downscaling purpose 134 stations that cover the period 1958–2000 are used to allow for an independent validation of the SD models.

Large-scale climate information was obtained for the period 1958–2000 from the 40-yr European Centre for Medium-Range Weather Forecasts (ECMWF) Re-Analysis (ERA-40) products (Uppala et al. 2005). The data were downloaded from the Asia–Pacific Data-Research

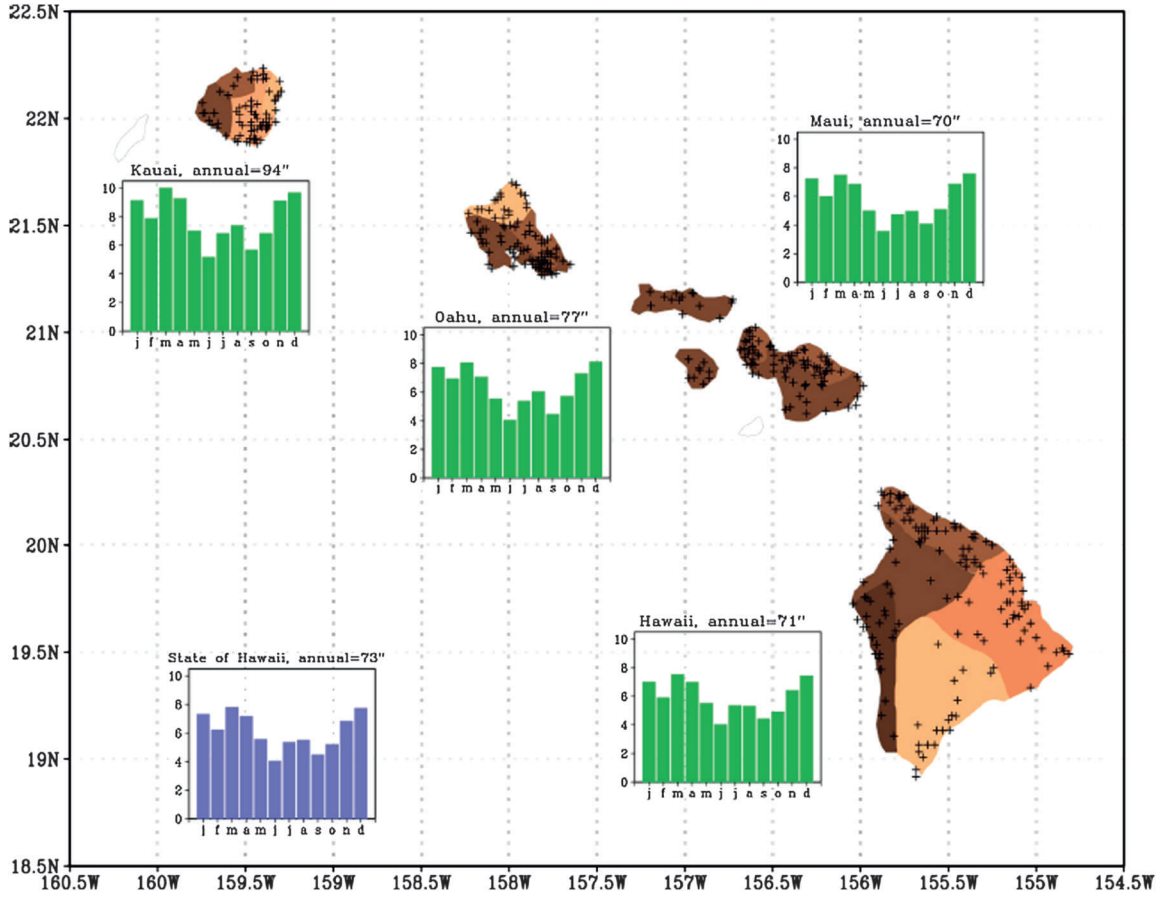

FIG. 1. Average monthly precipitation for the main Hawaiian Islands (inches). Averages calculated for the period 1921–80 based on 488 precipitation reporting stations. The state annual average (73 in. or 1854 mm) is a weighted average of the island means.

Center (APDRC) server (http://apdrc.soest.hawaii.edu/). The AR4 twentieth-century climate model simulations and the twenty-first-century A1B emissions scenario data were obtained from the FTP server (ftp-esg.ucllnl.org) that is maintained by the Earth System Grid II (ESG) research project sponsored by the U.S. Department of Energy Office of Science. We worked with a total of 21 models shown in Table 1.

a. Diagnostic analysis: Calibration and validation of the SD model

In this study a composite analysis is used for the synoptic classification of the large-scale circulations that are associated with either very dry or very wet months at individual stations in Hawaii. For each station the monthly mean rainfall data 1958–2000 were divided into two seasonal subsets (n = 258), the wet (November–April) and the dry (May–October) seasons, and sorted by increasing precipitation amounts. For each station the lower and upper 5% of monthly values were identified and the associated dates (i.e., month and years) provide the basis to form composite maps of the large-scale circulation.

We concentrate our analysis on a key region around Hawaii (10°S–40°N, 120°W–180°E). This region is assumed to be wide enough to contain sufficient large-scale climate information relevant to Hawaii's rainfall. A thorough objective criterion that would identify the optimal domain size for the downscaling purpose has not been attempted in this study. A smaller domain would give more weight to the regional aspects of the interacting large- and local-scale processes. This results in limited degrees of freedom for the SD. A limited domain size, however, reduces the risk of incorporating model biases from remote regions during the downscaling process. Thus, a compromise has to be made between the inclusion of biases and the loss of valuable predictor information (Kang et al. 2007). We note that the extension of the region across the equator helps to include the atmospheric imprints of El Niño and La Niña events over the eastern tropical Pacific. The northern latitudes in our domain allow us to include

TABLE 1. List of IPCC AR4 models that are analyzed in this study. Models that are selected for the SD of the twenty-first-century A1B scenarios are denoted with a superscript plus symbol. Note that the wind field data used in the downscaling were not available from those marked with an asterisk. Equilibrium climate sensitivity values are from Table 8.2 in Solomon et al. (2007). See Table 8.1 in Solomon et al. (2007) for model references.

No.	Reference letter	Model	Equilibrium sensitivity (K)
1	a	CCCMA_CGCM3_1$^+$	3.4
2	b	CCCMA_CGCM3_1_T63	3.4
3	c	CSIRO_MK3_0	3.1
4	d	GFDL_CM2_0$^+$	2.9
5	e	GFDL_CM2_1$^+$	3.4
6	f	GISS_AOM	N/A
7	g	GISS_MODEL_E_H	2.7
8	h	GISS_MODEL_E_R	2.7
9	i	IAP_FGOALS1_0_G	2.3
10	j	INGV_ECHAM4*	N/A
11	k	INMCM3_0	2.1
12	l	IPSL_CM4	4.4
13	m	MIROC3_2_HIRES	4.3
14	n	MIROC3_2_MEDRES	4.0
15	o	MIUB_ECHO_G*	3.2
16	P	MPI_ECHAM5$^+$	3.4
17	q	MRI_CGCM2_3_2A$^+$	3.2
18	r	NCAR_CCSM3_0	2.7
19	s	NCAR_PCM1	2.1
20	t	UKMO_HADCM3$^+$	3.3
21	u	UKMO_HADGEM1*	4.4

information related to the Pacific decadal oscillation (PDO).

With regards to the dynamics of the large-scale circulation, we concentrate the diagnostic analysis onto variables that can serve as predictors for the twenty-first-century downscaling pursuit. Based on our understanding that the low-level wind regime has a profound effect on mean rainfall over the islands, and that much of the monthly, seasonal, and interannual climate variability in the upper atmosphere is linked to changes in the low-level circulation (Sanderson 1993; Held and Soden 2006), we concentrate on near-surface variables in this study. The close connection between station rainfall, low-level winds, and upper-level circulation was initially tested with multiple linear regression, canonical correlation analysis and maximum covariance analysis (not shown). All these results demonstrated that the near-surface (1000 hPa) meridional wind component can explain a significant fraction of the precipitation anomalies throughout the islands. It was also found that additional low-level variables [zonal wind, sea level pressure (SLP)] add little independent information in addition to the meridional wind field. Other variables such as precipitable water and 500-hPa geopotential are highly correlated with the meridional wind field. Therefore they bring limited independent information into the SD model. Other factors are known to have a strong control on the rainfall over Hawaii: the strength and height of the trade wind inversion layer (Cao et al. 2007) and the vertical velocity in the 850- to 700-hPa level. The former diagnostic is not immediately available from the IPCC AR4 database. Limited data were available for the vertical winds and we therefore decided to focus on the meridional wind field component in this study.

The composite analysis identifies the typical circulation pattern that occurs during the driest and wettest months at one station. The difference between the associated meridional wind fields of the lower and upper 5% rainfall months is used as a projection pattern for the 1958–2000 ($n = 258$) monthly mean v-wind fields from the ERA-40 data. Note that in this step we take advantage of the larger sample size and work with monthly mean data instead of seasonal mean data ($n = 43$). The resulting index time series measures the similarity of the individual monthly mean v-wind field with the composite pattern. The station rainfall data are then converted into relative rainfall values {[(p − pmean)/pmean]100 (%)} at each station. The relationship between the station rainfall and the projection indices from the v wind is estimated with ordinary linear regression. For the calibration of the SD model, we decided to estimate the linear regression between seasonal means of the station rainfall data and the v-wind projection indices. The use of seasonal data was favored because of our basic interest in seasonal mean rainfall changes during the twenty-first century. The confidence

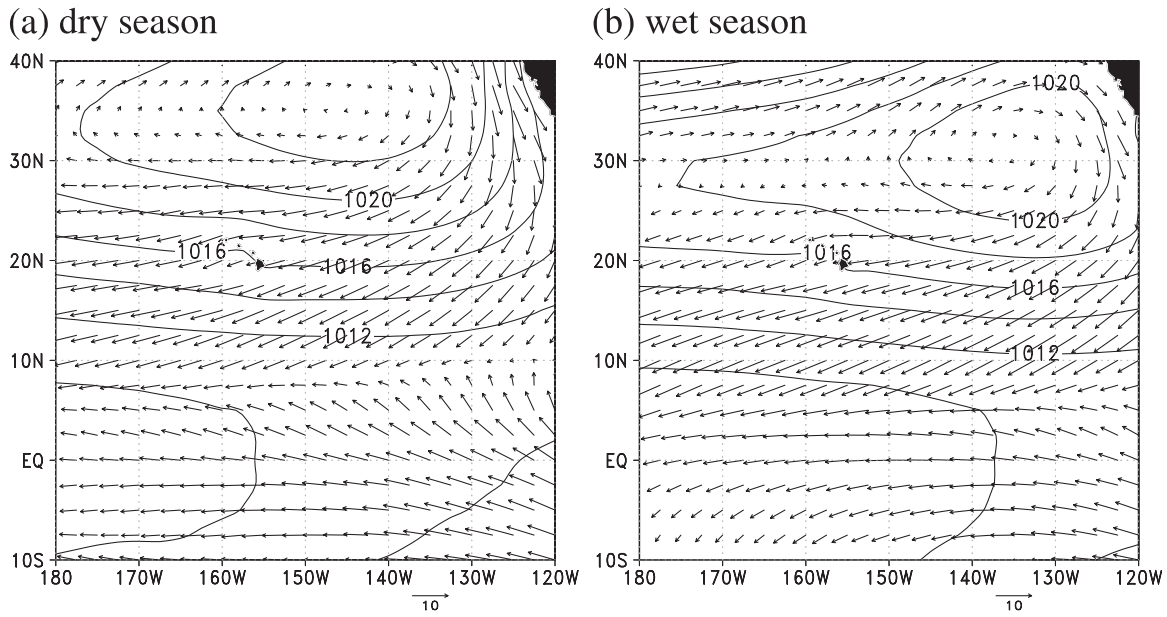

FIG. 2. Climatological SLP field and wind field in 1000 hPa for (a) the dry season and (b) and wet season averaged over 1970–2000. Data are from ERA-40 (Uppala et al. 2005).

intervals (von Storch and Zwiers 1999, p. 154) of linear regression are calculated during the calibration step. These take the uncertainty of the regression coefficients and the uncertainty of the residual error into account. Since the regression line will be applied to 30-yr averages of the AR1 scenarios, the uncertainty of the residual variance is scaled with a factor of 1/30.

The validation of the regression models follows the idea of dividing the observational data into a calibration and validation period (Michaelsen 1987). In this study, a moving window with a width of 21 yr is applied starting with the calibration interval 1958–78. The window is shifted by one year until it covers the period 1980–2000. The years outside the calibration window are used to compare the station rainfall with the estimates of the linear regressions. Explained variances (R^2_{cal}, R^2_{val}) were calculated to test the robustness of the linear relationships. After validation of the linear regressions, the IPCC's twentieth–twenty-first-century simulations are projected onto the diagnosed difference pattern (from the composite analysis) and the linear regressions are used to estimate the corresponding rainfall anomalies that are expected from the wind changes at the end of the twenty-first century (i.e., difference mean 2070–99 minus mean of 1970–2000).

b. Analysis of model skills

To find a quantitative measure regarding which models should be included in our study of the twenty-first-century rainfall projections for Hawaii, we analyzed the fields of the twentieth-century climate simulations (20c3m) to select the ''best'' models. This analysis was carried out over the region 10°S–40°N, 120°W–180°. The SLP field was used. The decision process is guided by a visual selection process. We refrain from a more formal development of an objective metric for our specific SD pursuit.

Three different criteria were tested for each model for the wet and dry season:

1) How well is the SLP field represented in the models compared with the ERA-40 climatology (1970–2000)?
2) How well is the spatiotemporal variability reproduced in the models?
3) Does the variance of the meridional wind component match the observed ERA-40 variance?

The differences in the mean are measured in terms of the mean absolute error (MAE):

$$\text{MAE}(k) = \frac{1}{n}\sum_{ij} \left| x_k(i,j) - x_r(i,j) \right|, \qquad (1)$$

where i, j are indices for the longitude and latitude of the n grid points; $x_k(i, j)$ is the SLP of model number k; $x_r(i, j)$ is the ERA-40 SLP (see Fig. 2). Note that one could also work with the root-mean-square error (RMSE) (e.g., Taylor 2001) but the MAE gives less weight to outliers.

For the spatiotemporal variability comparison, the SLP fields 1970–2000 from ERA-40 and the models were subject to an EOF analysis. The leading $m = 10$

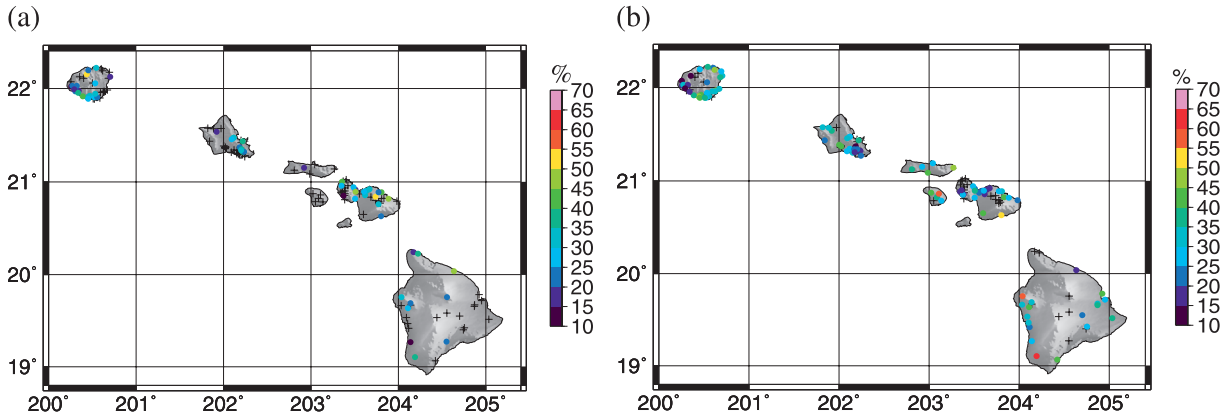

FIG. 3. Explained variance (%) for each station-based regression model: (a) the dry season, (b) the wet season. Note that stations without statistically significant ($p = 5\%$) linear correlation are marked with black crosses.

spatial eigenvectors and the explained variances were used to define an EOF skill score (ESS) according to

$$\mathrm{ESS}_k = \frac{\sum_i^m \sum_j^m w(i,j)\left|r_k(i,j)\right|}{\sum_i^m \sum_j^m w(i,j)}. \qquad (2)$$

In Eq. (2), the correlations $r_k(i, j)$ between ith spatial EOF pattern of model k and the jth EOF of ERA-40 are summed over a limited range of EOF combinations. Since EOF analyses often result in pairs of equally important modes (North et al. 1982), the skill score gives weight to spatially correlated modes that are offset by one rank using the weight function

$$w(i,j) = \begin{cases} 0.5\sqrt{\lambda_k(i)\lambda_r(j)} & : \quad i = j-1 \\ 1.0\sqrt{\lambda_k(i)\lambda_r(j)} & : \quad i = j \\ 0.5\sqrt{\lambda_k(i)\lambda_r(j)} & : \quad i = j+1 \\ 0 & : \quad \text{elsewhere} \end{cases}, \qquad (3)$$

with i, j representing the EOF modes $1, \ldots, m$. The weights in the EOF skill score ESS_k also account for the explained variance $\lambda_k(i)$ and $\lambda_r(j)$ of the eigenmodes of the model and the reanalysis, respectively. This heuristically derived measurement summarizes the information that is shown for illustrative purposes in next section (Fig. 10). A perfect correspondence of the spatial EOF modes in the model compared with ERA-40 would result in a skill score of 1 (note that the minimum skill score is 0).

Finally, it is crucially important for the statistical projection purpose that the variability in the meridional wind field of ERA-40 and the models are locally of similar magnitude during the twentieth century. A bias in the interannual-to-decadal variance may also distort the projected changes in the wind fields and, ultimately, the projected rainfall anomalies.

One way to measure the model skill of reproducing the observed variability in the wind is the average over the logarithmic ratios between the reanalysis and the modeled variance at each grid point in the study area:

$$\mathrm{MLV}_k = \frac{1}{n}\sum_{i,j} \log\left\{\max\left[\frac{v_k(i,j)}{v_r(i,j)}, \frac{v_r(i,j)}{v_k(i,j)}\right]\right\}, \qquad (4)$$

where the indices i, j correspond to the n spatial grid points. The mean logarithmic variance (MLV) is a nonnegative value. A perfect match between modeled and reanalysis variability would result in an MLV_k of zero. A value of 1 would indicate that the variance ratio is on average an order of magnitude different. The maximum function avoids cancellation effects if models show regions of both underestimated and overestimated variance.

3. Results

a. *Observed relationship between large-scale circulation and rainfall*

This section addresses the question of how the large-scale circulation is related to the station-based precipitation on the islands of Hawaii. The aim is to identify which locations on the islands are predominantly controlled by large-scale circulation anomalies. The dynamical structure of circulation modes are analyzed and serve as a "proof of concept" for the SD approach.

After applying the composite analysis (see methods) to the 1000-hPa winds for the individual station rainfall data, the v wind from ERA-40 is projected onto the associated anomaly composite pattern. The resulting index time series are regressed onto the associated

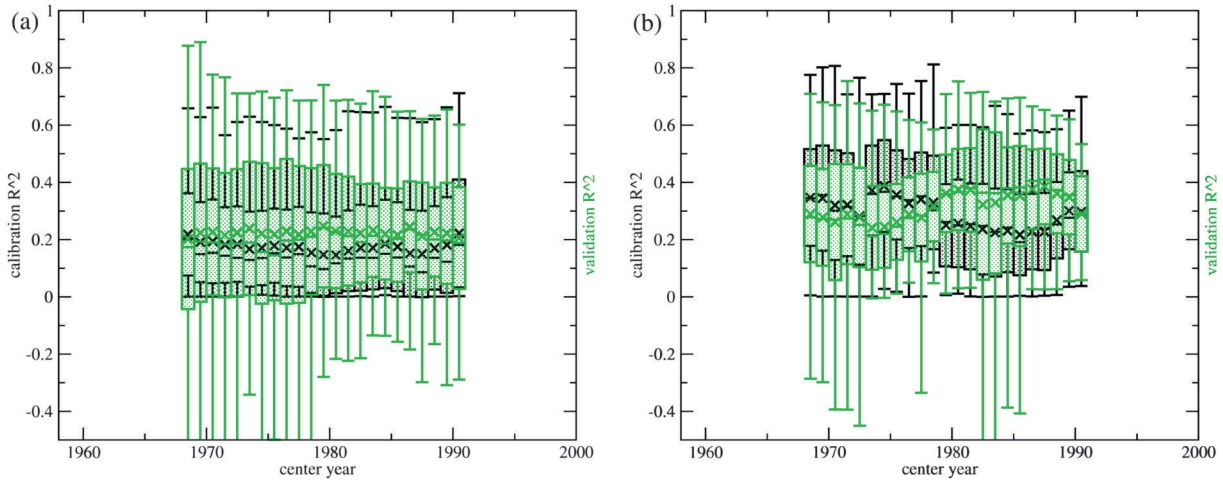

FIG. 4. Explained variances of the calibration (R^2_{cal}, black) and validation [sgn(R_{val})R^2_{val}, green] intervals using a 21-yr moving window for calibration and the remaining years for the validation of the linear regressions: (a) dry season 1958–2000; (b) wet season 1958–2000. The box and whiskers plots show the median, standard deviation, minimum, and maximum values of the squared correlations between the 134 stations' rainfall and their corresponding v-wind indices. Black (green) crosses denote the station-mean R^2_{cal}[sgn(R_{val})R^2_{val}] values for each data window. Note that all stations with sufficient data (10 seasonal rainfall values) were included irrespective of the statistical significance of their R_{cal} values. Center year refers to the center of the 21-yr calibration window.

relative rainfall anomalies. Here, the wet/dry seasons of the years 1958–88 are used for the calibration of the linear regression parameters. The correlations between the individual rainfall time series and the v-wind indices show that a significant amount of the rainfall variability is controlled by the winds, especially during the wet season (Fig. 3b). The spatial distribution further indicates that the SD can be applied to both the windward and leeward sides of the islands. However, the statistical relation between the wind field and the rainfall is weaker in the dry season (Fig. 3a). Weaker correlations during the dry summer month were expected, since few sporadic and localized heavy rainfall events have more influence on the seasonal mean precipitation.

To test the predictive skill of the calibrated linear regressions, the observational period 1958–2000 was divided into nonoverlapping calibration and validation intervals (see section 2). Although individual stations can show very different validation results, the average over all stations indicates reasonable R^2_{val} values (Fig. 4). It must be noted that the validation of the regression models serves as a means to lend credence to the application of the SD to future climate change. Aside from low amounts of explained variability, large discrepancies between R^2_{cal} and R^2_{val} are indicators of nonstationarity in the case of ordinary linear regressions. The climate shift in the 1970s that was identified in many climate records over the Pacific (Trenberth 1990; Miller et al. 1994; Gedalof and Smith 2001; Meehl et al. 2009) could have served as an ideal test environment for the SD method (Wang and Zhang 2008). However, the validation is sensitive to changes in the data quality of the reanalysis products and the station data. Advances in remote sensing significantly improved the reanalysis products beginning in the 1970s. Systematic increase in data gaps in the station network during the late 1970s and 1980s change the number of samples in validation and calibration windows. All these factors contribute to differences between the explained variances of the calibration and validation. Over all, the validation shows that the calibration statistics provide a reasonable estimate of the predictive skill. Only stations with

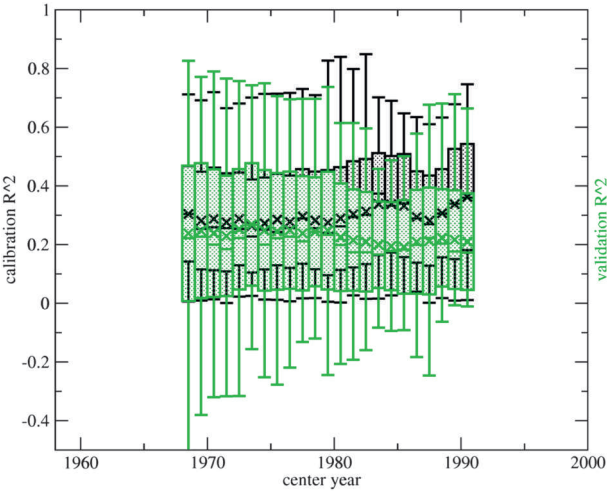

FIG. 5. Explained variances of the calibration (R^2_{cal}, black) and validation [sgn(R_{val})R^2_{val}, green] as in Fig. 4a but with the projected ω_{700} indices as an additional predictor to the v-wind indices.

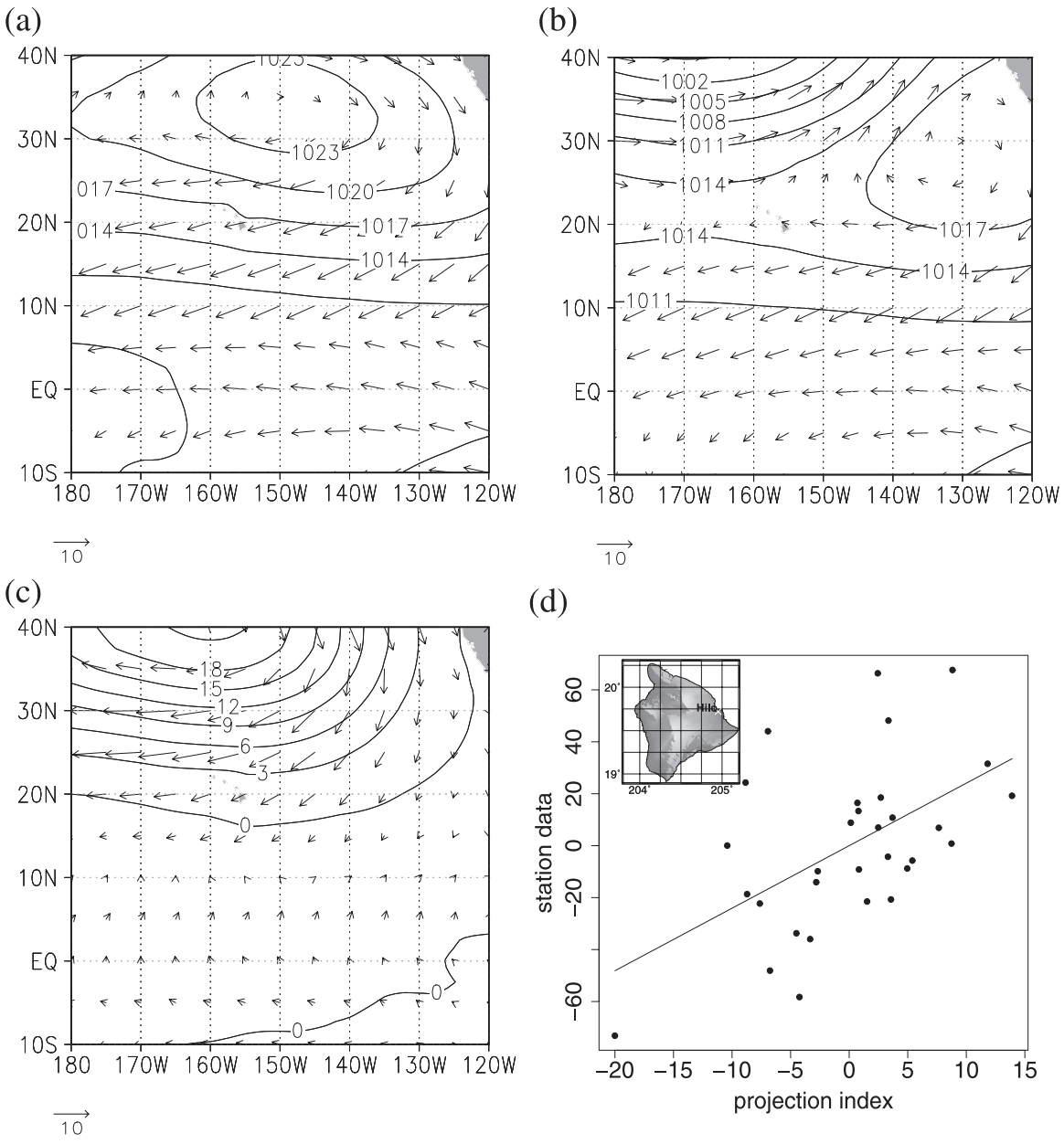

FIG. 6. Composite analysis of the SLP and 1000-hPa wind for the high- and low-precipitation winter months at station Hilo on the Big Island during 1958–2000 ($n = 258$): (a) the mean circulation averaged over the months associated with the p_{95} quantiles of the monthly mean rainfall data; (b) the average circulation for the month with lowest rainfall (p_5 quantile); (c) difference of the mean circulation high–low composite. (d) The seasonally averaged meridional wind field index (see text for details) associated with the difference field in (c) is regressed onto the rainfall data (percent anomalies) from station Hilo, 1958–88 ($n = 31$, $r^2 = 0.29$).

sufficient sample size (minimum of 10 seasonal rainfall estimates) and with a significant ($p = 5\%$) statistical relationship were used for the final downscaling of the scenarios onto the station rainfall (section 3c). This resulted in a reduction to 97 (57) out of 134 rainfall stations suitable for the downscaling in the wet (dry) season. In the following, we decided to use 1958–88 as the calibration period for the linear regression models.

We also applied the vertical velocity fields in 700 hPa (ω_{700}) as a predictor for the dry-season rain. The station-averaged correlation between dry-season rainfall and ω_{700} is similar to the one obtained with the v wind. In case of v wind and ω_{700} as predictors, the overall correlation was not increased (Fig. 5). The latter result is an indicator of multicollinearity in the predictor variables. Physically, the statistical results suggest a close

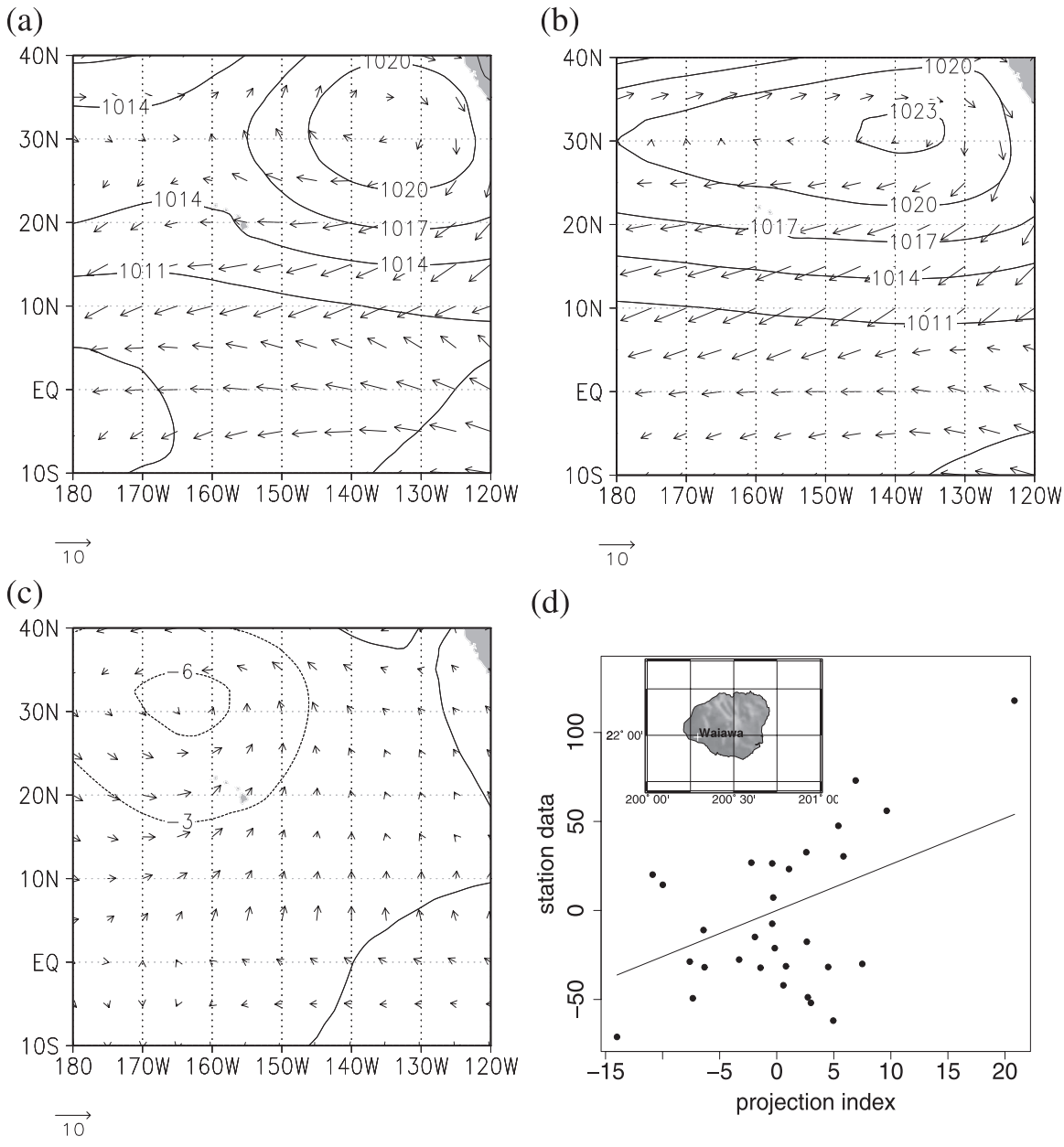

FIG. 7. Same as Fig. 6 but for the station Waiawa on the leeward side of Kauai. Note that the linear regression results in a significant correlation ($n = 31$, $r^2 = 0.17$).

connection between the horizontal winds (i.e., convergence) and the vertical motions above.

The composite analysis of the 134 stations showed two dominant modes in the v-wind field. To illustrate the dynamical structure of these modes, composites of zonal winds and SLP were calculated in addition to the v wind. Figures 6 and 7 depict the composites for Hilo on the Big Island and Waiawa on Kauai, respectively. The wet-season rainfall at Hilo has a correlation ($R^2_{\text{cal}} = 0.29$) with the v-wind index 1958–88 ($n = 31$). The composite maps of the ERA-40 SLP and 1000-hPa wind field show that a more pronounced subtropical high northeast of the islands produces stronger northeast trade winds that favor the formation of rainfall.

Negative precipitation anomalies are observed during seasons when the high pressure cell and the trade winds are weaker than average. Despite the stronger low pressure systems in the North Pacific, the contribution from frontal rain systems cannot compensate for the reduction in trade wind–induced rainfall. The majority

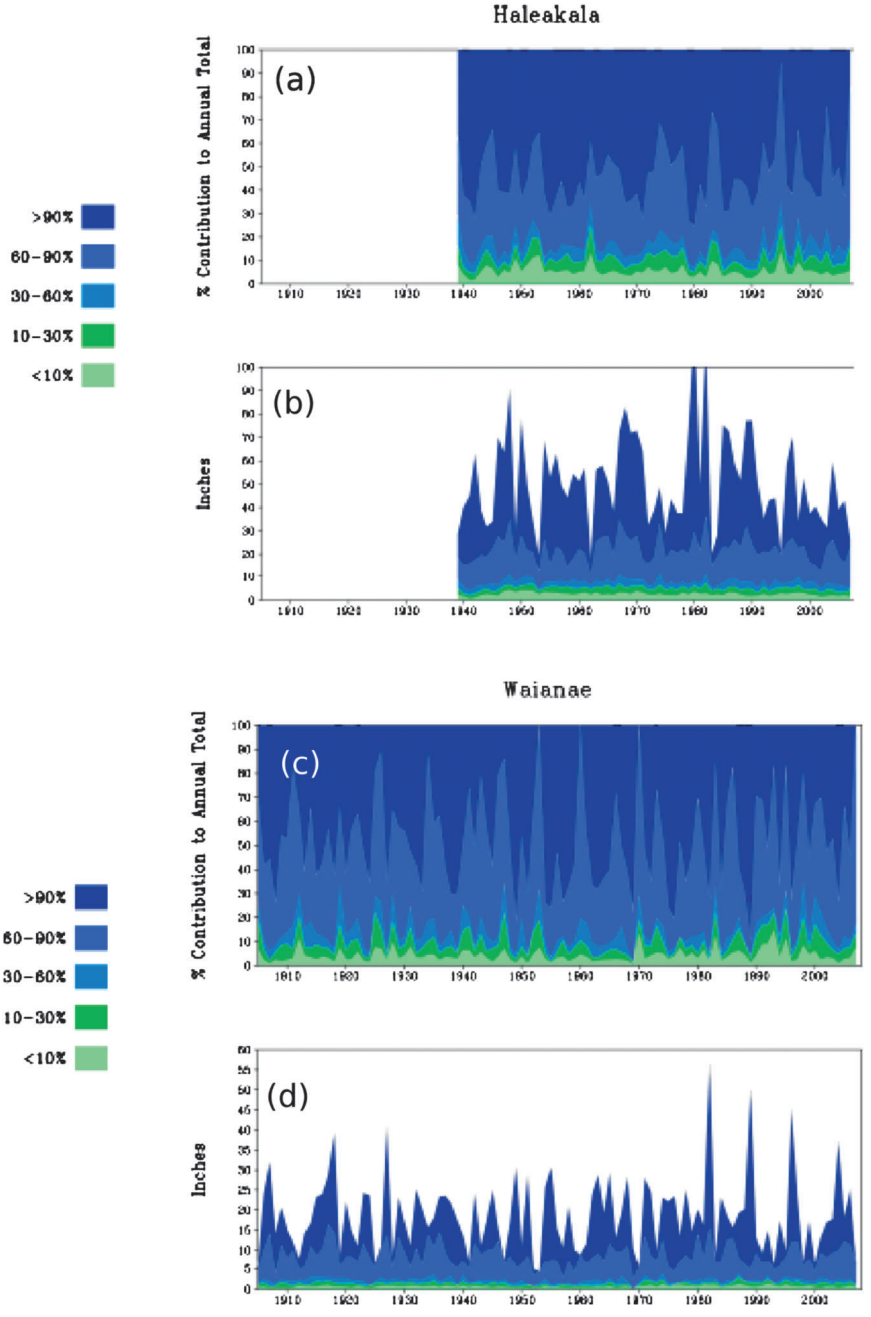

FIG. 8. Time series of annual rainfall at (a),(b) Haleakala, Maui, and (c),(d) Waianae, leeward coast of Oahu for respective periods of record. (b) and (d) give the annual rainfall totals as contributed by the daily events, in terms of their magnitude (quantile value). (a) and (c) give the percentage contribution to each annual total by these quantiles.

of the windward sites on the islands fall into this trade wind–related rainfall regime (Woodcock 1975; Lyons 1982; Sanderson 1993; Chu and Chen 2005).

At Waiawa, a station on the leeward side of Kauai, the v-wind field explains 17% of the wet-season rainfall variability (Fig. 7). The rainfall is associated with kona lows west-northwest of the islands. The resulting southerly winds advect warm moist air masses toward the islands. This synoptic weather pattern occurs less frequently than the trade wind regime, but it can cause intense rainfall events over the islands. Figure 8 gives two rather typical examples of the contribution by

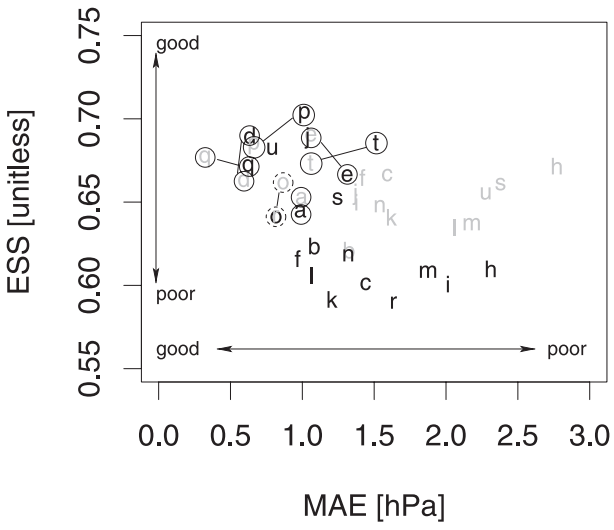

FIG. 9. Skill score statistics of the AR4 models: bias in the 1970–2000 mean SLP field in the region 10°S–40°N, 120°W–180° is measured as the MAE (in hPa); spatial correlation of the leading EOF modes in the 1970–2000 SLP field over the same region [Eq. (2)]. Reference climatology and EOF modes were analyzed from the ERA-40 data 1970–2000. Black (gray) letters mark the wet (dry) season. See Table 1 for model identification. The AR4 models selected for the twenty-first-century rainfall projection are marked with solid circles. Note that our selection criteria would also favor model "o" (dashed circle), but data were not available for the twenty-first century.

different climatological quantiles of the observed daily rainfall to the annual totals for Wainanae on the leeward side of Oahu and Haleakala, Maui. The plots show for each year of record the amount of annual rainfall associated with different quantiles from the daily rain probability density function (PDF) (Figs. 8b,d) and the percentage contributions to each annual total (Figs. 8a,c). The upper 10% of all daily rainfall events account for 50% or more of the annual totals. Therefore, the lower correlation observed in Fig. 7d with the large-scale wind field is consistent with the physical mechanisms of rainfall generation.

b. GCM evaluation

The model evaluation is based on the comparison between the ERA-40 climate and individual AR4 twentieth-century scenario runs (years 1970–2000). The objective quantification of the model skill is evaluated in the region around Hawaii (10°S–40°N, 120°W–180°). SLP and the v wind in 1000 hPa are analyzed. Based on the three test criteria (see section 2) and data availability this screening procedure reduces the number of GCMs from 21 to 6, which are used in the final SD step.

First, the differences in the climatological mean SLP are analyzed for the wet and dry season. The MAE [Eq. (1)] ranges from 0.5 to 3.0 hPa, without any seasonal dependence (Fig. 9). Second, the spatial correlation between the dominant EOF modes in the SLP field gives a quantitative measure of the models' ability to reproduce the interannual-to-decadal variability around the Hawaiian Islands and extratropical–tropical teleconnection regions (see Fig. 9). To illustrate the meaning of the ESS [Eq. (2)], Fig. 10 represents two examples of the spatial correlation matrix derived from the leading 10 EOF modes. The better the spatial agreement in the EOF modes and the better the agreement in the ranks of these EOFs, the closer are the values with high correlation aligned along the diagonal. The two given examples correspond to models (q and u in Table 1) with a good correlation with the ERA-40 EOF modes.

The information contained in Fig. 10 is represented in the ESS [Eq. (2)] and Fig. 9 shows the results for the AR4 models. The models are generally of equal quality in terms of EOF modes during the summer season (gray symbols in Fig. 9). During the winter months, a group of models reveal markedly lower skills. Together with the differences in the mean SLP fields and the requirement of equally good performance in the wet and dry seasons, we used Fig. 9 as a guide and selected 6 out of the 21 AR4 models for the rainfall projection purpose. It must be noted that for model o (see Fig. 9) the meridional wind field was not available at the time of our analysis. Furthermore, the third criterion, which measures the local variance ratios of the v wind between models and reanalysis, showed that the selected models are in a reasonable variance range (Fig. 11).

c. Projected climate change and rainfall change

In this section, the projected changes in the v-wind component and the regressed Hawaiian rainfall anomalies are presented. We will address to what extent the models project the same large-scale circulation changes and what the expected rainfall anomalies from these wind changes are. The projected rainfall changes are based on the linear regressions between the v-wind field and the seasonal rainfall data that were developed in the previous section (section 3a). Only stations that passed the statistical significance test are used for purposes of downscaling the AR4 projections.

In Fig. 12 the differences between the end of the twenty-first-century (2070–99) and the late-twentieth-century (1970–99) averages for the wet-season circulation are depicted for the selected models. The largest differences are projected in simulations q and t (Figs. 12e,f). For model t, the v-wind anomalies indicate a stronger northerly wind northeast of the islands and anomalous southerly winds in the equatorial region.

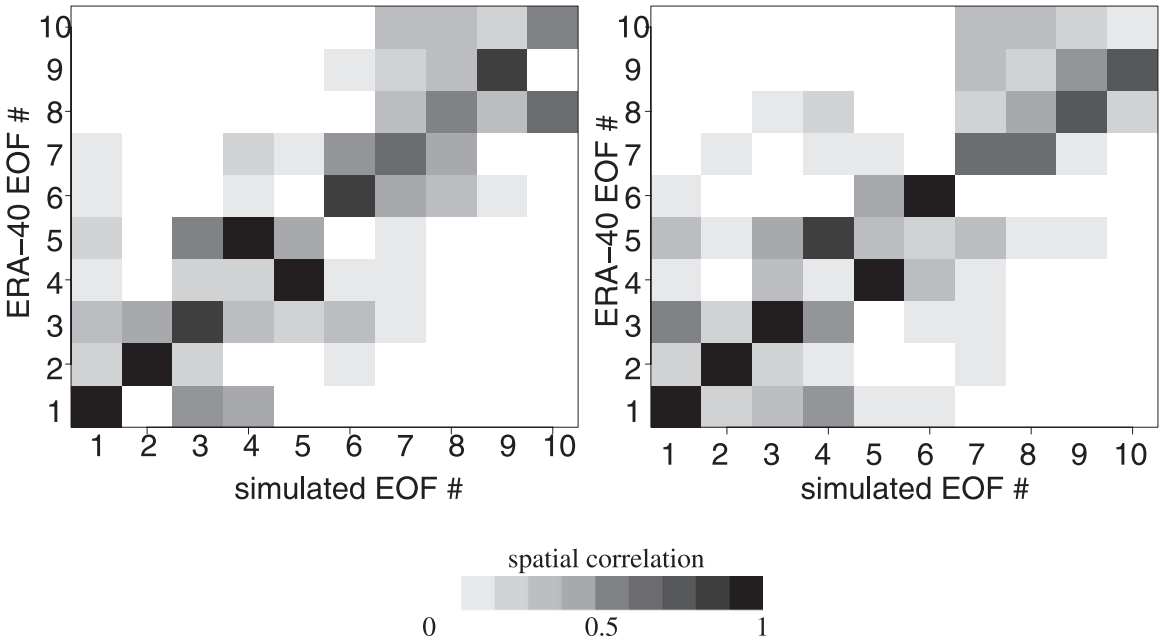

FIG. 10. Matrix of the spatial correlation among the leading 10 EOF eigenmode pattern of the SLP field from the ERA-40 data and two AR4 models. Color shading indicates the correlation. The higher the concentration along the diagonal axis, the better the agreement in the spatial eigenmodes between the model and ERA-40. (left) Model q; (right) model u (see Table 1).

The slight positive wind anomalies above the islands and northerly anomalies west of the islands are the result of an SLP anomaly that resembles a cyclonic circulation northwest of the islands. The v-wind pattern resembles both a strengthened trade wind regime and an enhanced kona low activity. In contrast, the change in the v wind simulated by model q shows almost the inverse anomaly pattern. The most pronounced changes appear in the equatorial region. Weaker trade winds and an anomalous northerly component in the equatorial regions that extend over the Hawaiian Islands are in clear contrast to the results of model t. The other model simulations show a smaller amplitude in the change of the v-wind field. In the ensemble average, the large

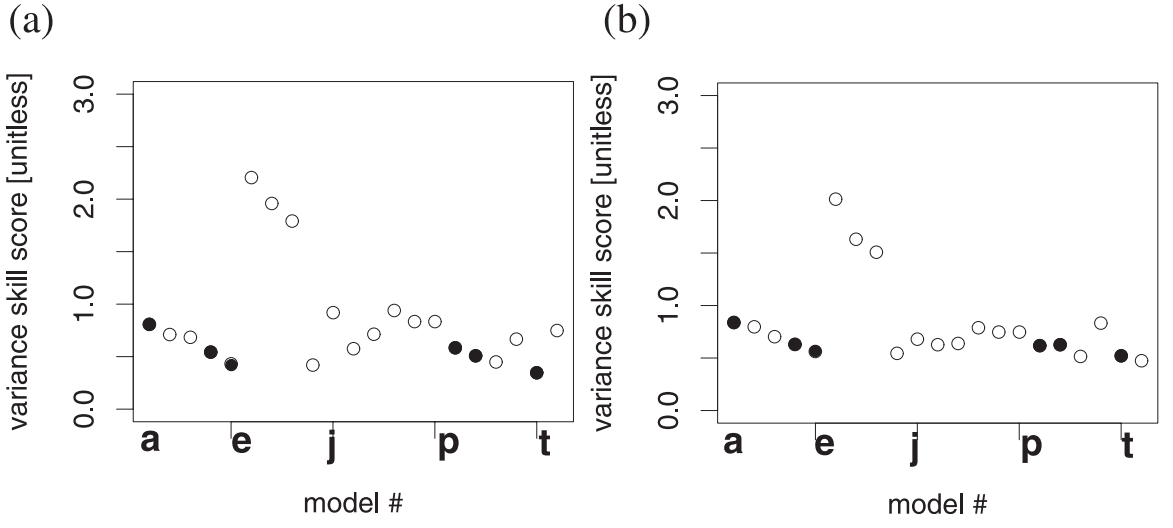

FIG. 11. Model skills in reproducing the observed ERA-40 interannual–decadal variability in the meridional wind field (1000 hPa) in the region 10°S–40°N, 120°W–180° during 1970–2000: (a) the wet season, (b) the dry season. Note that a perfect grid-by-grid match between observed and modeled variance would give a value of 0. See text for details. Filled circles mark the selected models for the downscaling analysis.

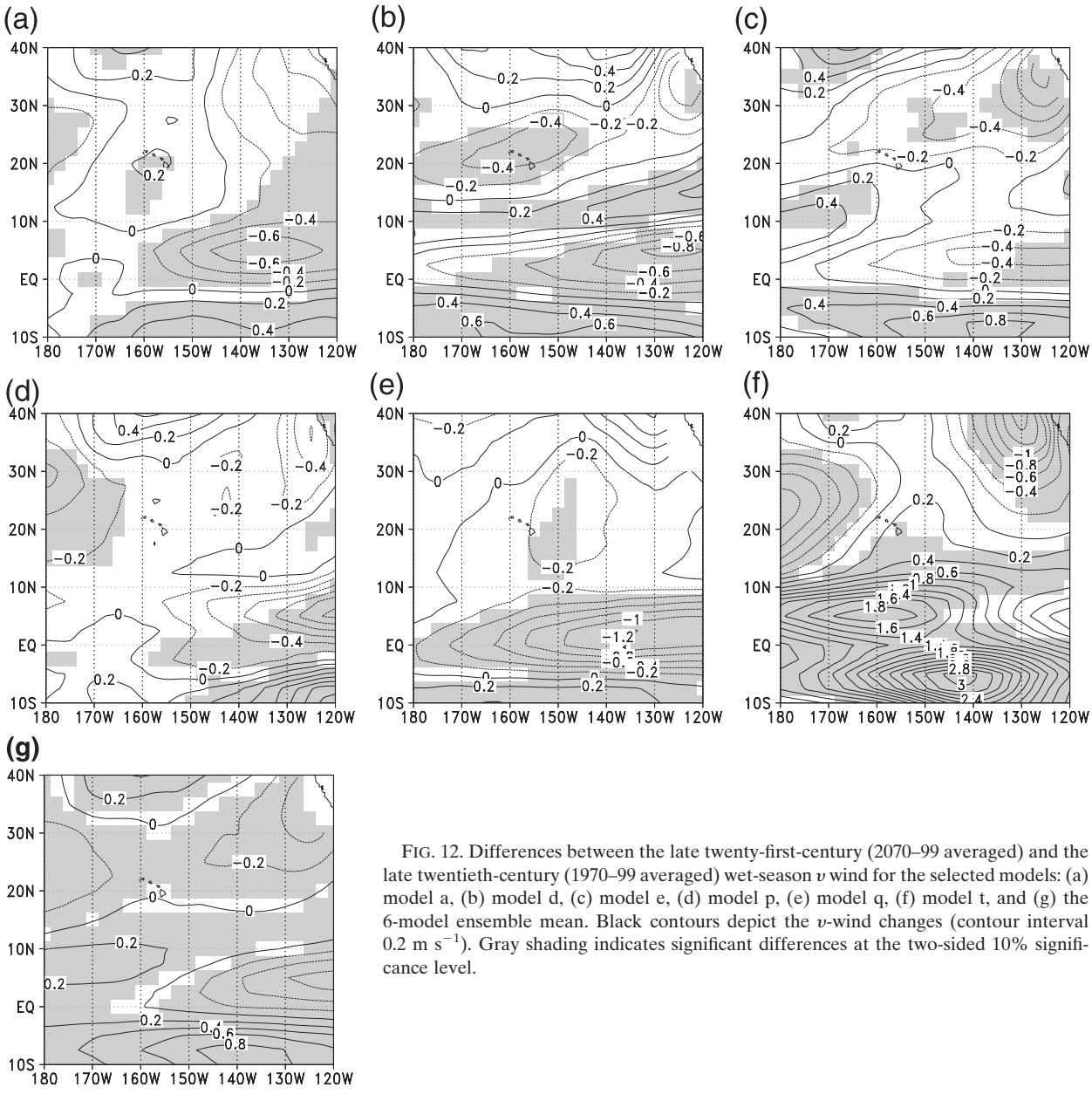

FIG. 12. Differences between the late twenty-first-century (2070–99 averaged) and the late twentieth-century (1970–99 averaged) wet-season v wind for the selected models: (a) model a, (b) model d, (c) model e, (d) model p, (e) model q, (f) model t, and (g) the 6-model ensemble mean. Black contours depict the v-wind changes (contour interval 0.2 m s^{-1}). Gray shading indicates significant differences at the two-sided 10% significance level.

amplitude changes cancel each other and the resulting wind anomalies are smaller, which makes a dynamical interpretation of the ensemble mean changes more ambiguous, despite their estimated significance (p = 0.1). The results further highlight that the different AR4 models locally project different wind changes over Hawaii, and their teleconnection to the tropics and extratropical centers of action are not robust among the models. This imposes a fundamental problem on the objective definition of the proper domain size for the SD.

Without discussing the details for the circulation changes during the dry season, it is noteworthy that model q and model t project similar wind anomalies during the dry season compared with the wet-season anomalies (Fig. 13). Largest wind anomalies occur over the equatorial regions in these individual models, but the ensemble mean shows only weak anomalies in the equatorial regions and south of the islands.

The projection of these simulated v-wind changes onto the station-related composite pattern provides the index values that are translated into projected rainfall anomalies at each station by application of the established regression lines. These downscaled scenarios of the late twenty-first century are plotted in Figs. 14–16 in

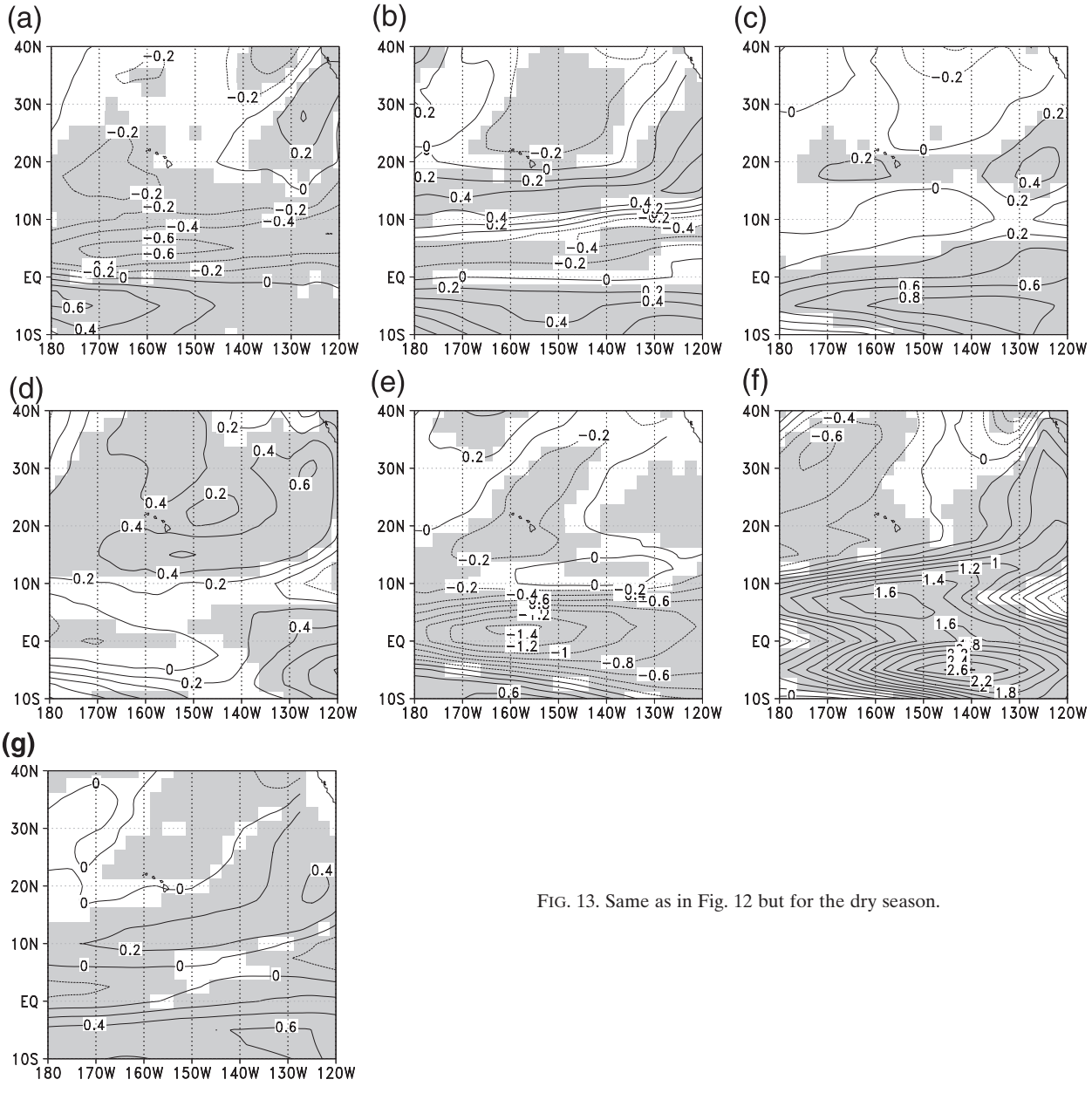

FIG. 13. Same as in Fig. 12 but for the dry season.

the form of relative precipitation change at each station. The estimated 2-sigma standard deviations (i.e., approx 95% confidence intervals) are also provided. As expected from the weak circulation changes depicted for the 6-member ensemble mean in Figs. 12g and 13g, the projected rainfall changes are low and do not exceed 20% at most stations. In the dry season (Figs. 14a–c), the ensemble mean projects slightly increased rainfall for northwest Maui, but the statistical uncertainties of downscaled rainfall anomalies are too large to draw affirmative conclusions about the projected regional rainfall changes. For the same reason, no important precipitation changes are found in the 6-model ensemble mean during the wet season (Figs. 14d–f). An increase along the west-facing coast of the Big Island is projected, but the statistical uncertainty (which includes the unresolved variability) is rather large. Since the individual models in the 6-member ensemble reveal some striking variations in their projected wind anomalies, Figs. 15 and 16 present the downscaled precipitation changes for the two models with the largest anomaly amplitudes, models q and t, respectively. In the dry season the local character of the precipitation is noticeable. On the northernmost island (Kauai), the two

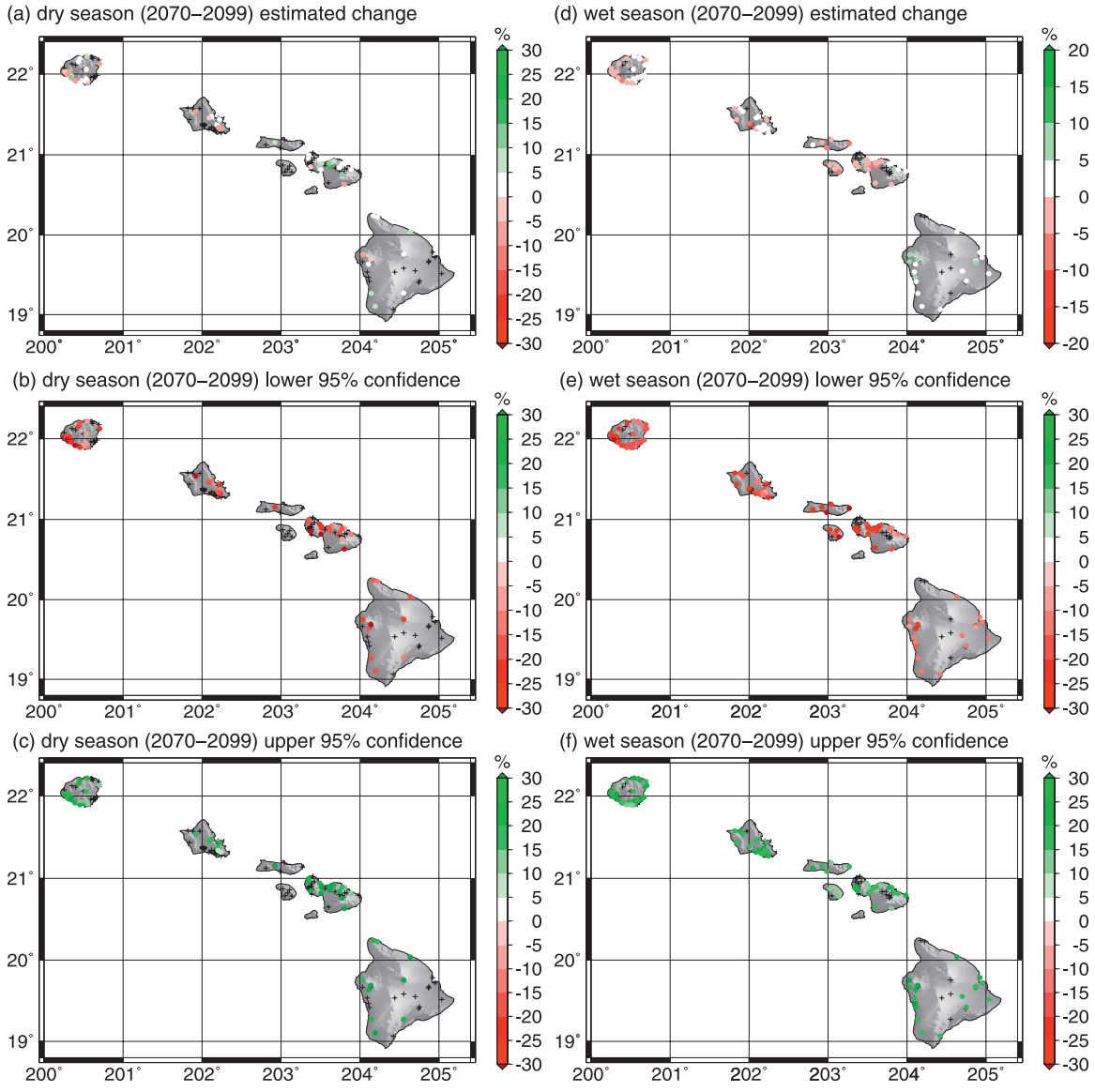

FIG. 14. Projected rainfall changes (anomalies with respect to the 1970–99 climatological mean in %) during the (a)–(c) dry and (d)–(f) wet season using the 6-model ensemble mean of the projected v-wind anomalies. (top) The maximum likelihood estimate. (middle) The estimated lower margin of the 95% statistical confidence interval. (bottom) The upper margin of the 95% confidence interval. See text for discussion of the statistical confidence interval. Note the varying color scales of the plots. Stations without a significant statistical relationship between rainfall and v-wind field (crosses) were not used in these estimates.

downscaling scenarios show pronounced regional gradients from wet to dry anomalies, however, with opposing signs between the two models. Over the Big Island, an east–west gradient is noticeable, but again the signs oppose each other in models q and t. During the wet season the effect of the large-scale circulation changes translates into a spatially more homogeneous pattern. Yet again, the two solutions derived from the wind anomalies provide two opposing scenarios for Hawaii: a dryer climate or a wetter climate. It should be noted that, for the majority of the stations, the percentage rainfall changes is below 30% and only a few locations indicate robust changes with regards to the statistical confidence ranges.

A more comprehensive description of the islandwide rainfall changes is given in form of a histogram. Taking the percentage changes at all stations and for all six model scenarios together, the number of stations falling into 5% bins is counted. The bimodality in Fig. 17b reflects the two opposing scenarios during the wet season. The maximum likelihood value suggests an islandwide 5%–10% rainfall decrease in the wet season. The

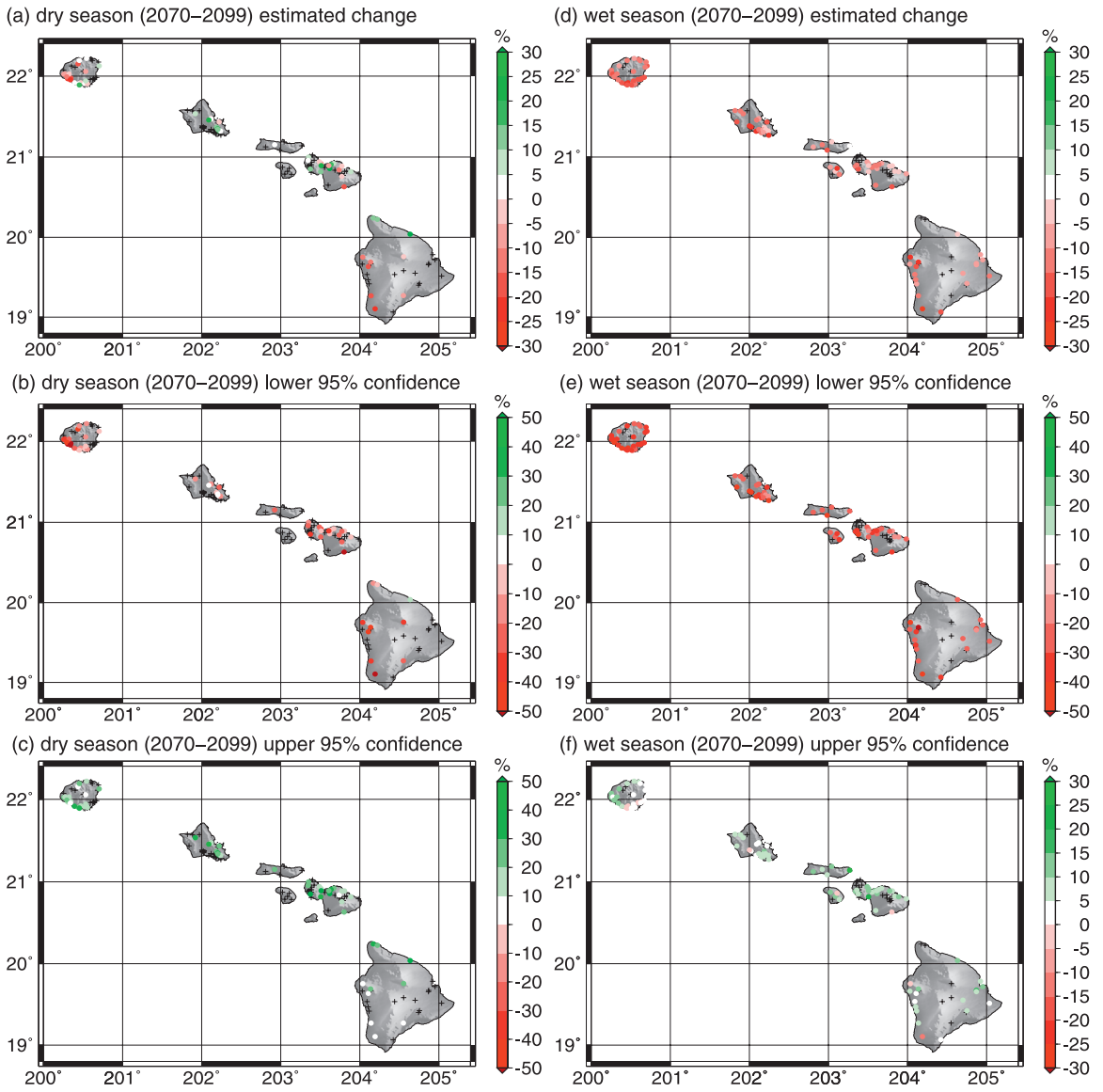

FIG. 15. Same as in Fig. 14 but for the projected rainfall anomalies using the v-wind anomalies from model q. Note the varying color scales of the plots.

histogram highlights the differences between the mean, median, and maximum likelihood estimate. Because of the bimodality, we prefer the value of 5%–10% rainfall decrease over the ensemble mean value (which is close to 0%). The histogram of the dry season is closer to a unimodal distribution. A 5% increase in rainfall over the islands is indicated as the maximum likelihood value.

4. Discussion and summary

The SD presented here is an attempt to exploit the dynamical linkage between the large-scale circulation and individual station rainfall on the Hawaiian Islands. Prior to this study very limited information was available for this remote region in the Pacific. The current state-of-the-art GCM models that have been used for the IPCC AR4 scenario runs have a coarse grid resolution of about 200 km × 200 km. In these models, the islands with their topographic features are not represented. The underlying work hypothesis for the SD procedure is that the missing physical processes (such as the topographic effect of the mountains on the trade winds) can be represented by statistical relationships.

In this case study only linear methods have been applied. We restricted our predictor information to the meridional wind in the lower atmosphere. Especially for

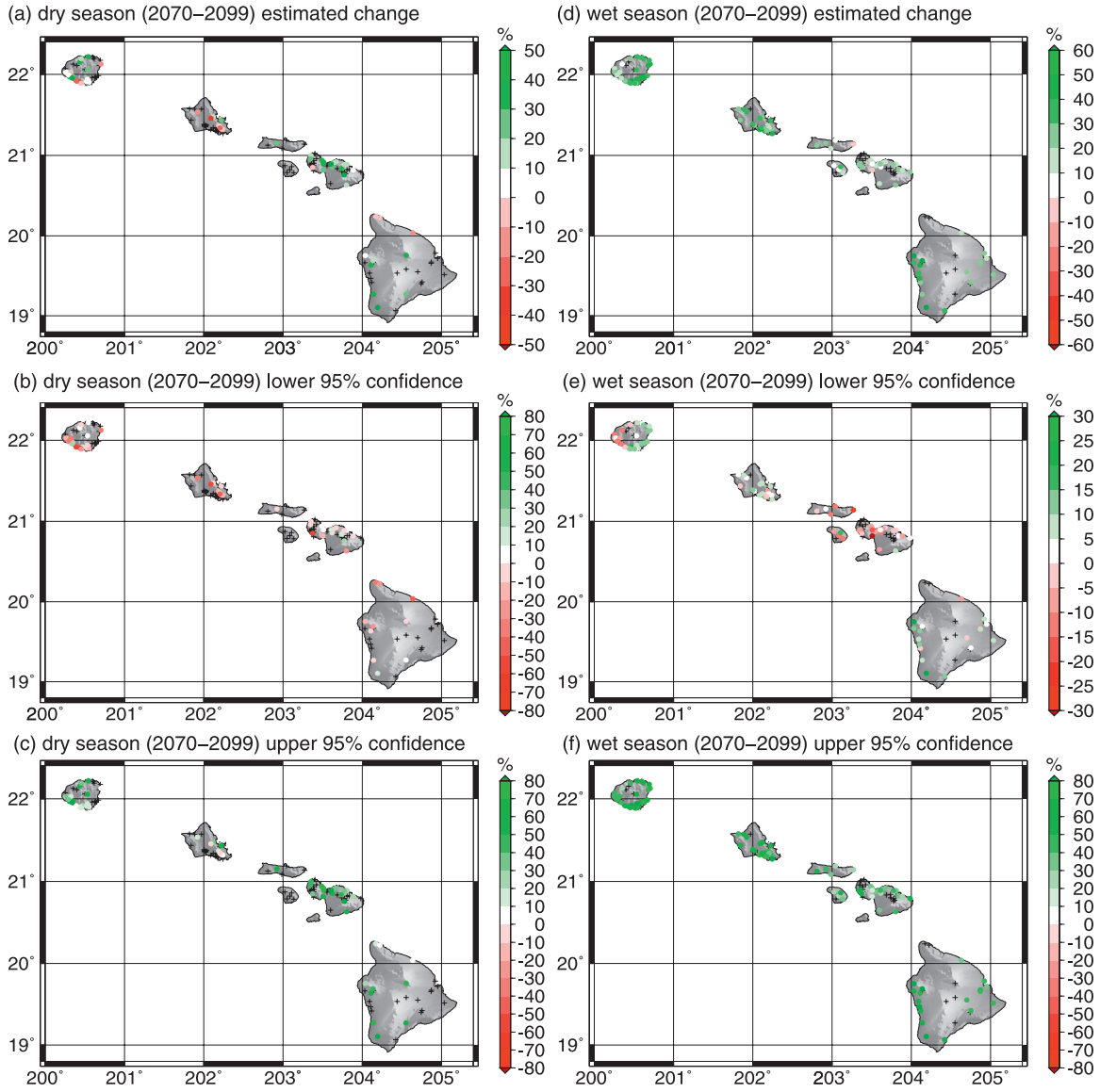

FIG. 16. Same as in Fig. 14 but for the projected rainfall anomalies using the v-wind anomalies from model t. Note the varying color scales of the plots.

the dry season and the dry regions of the islands, this approach has limited success. Future improvements will require additional information in the form of multivariate predictor climate fields. The height and strength of the trade wind inversion, vertical motions on the 700-hPa level, transient eddy activity, and low-level moisture convergence are fundamental control factors (Lyons 1982; Chu et al. 1993; Schroeder 1993; Cao et al. 2007). Therefore multivariate regression methods with these additional large-scale circulation characteristics are promising to improve the overall statistical projection skill. However, our first tests with the inclusion of the vertical winds at 700 hPa did not improve the overall predictive skills, though some regressions of individual stations profit from this extra information. A careful case-by-case analysis will be required in future.

The linear regression techniques are less suited to regions with long dry spells and few rain events in the seasons. Here, a few extreme synoptic weather events can bring the bulk of rainfall during the year (Fig. 8). A strong linear connection with seasonally averaged large-scale circulation fields cannot be expected to explain a large percentage of the local rainfall variability. Future downscaling methods must try to derive optimal nonlinear transformation functions between the predictors and the extreme rainfall (Wang and Zhang 2008). Since

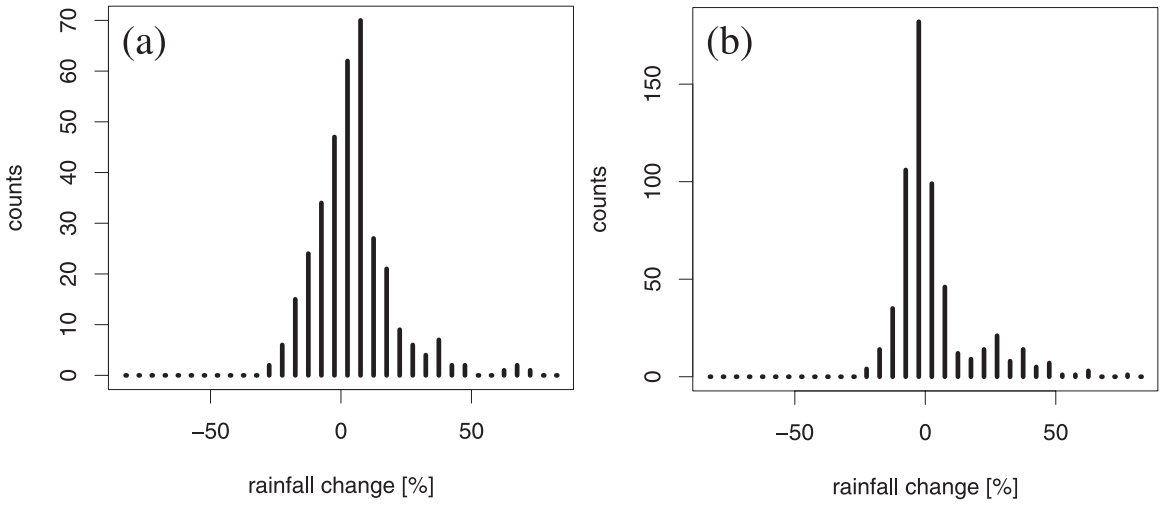

FIG. 17. Number of stations falling into each 5% bin of downscaled rainfall changes. Counts were summed over all six models. (a) Dry season and (b) wet season.

this study was the first attempt to downscale the projected twenty-first-century climate change scenarios onto Hawaiian rainfall, it was important to understand the linear statistical relations.

The 95% confidence ranges that were estimated for the projected rainfall changes serve as a guideline for the uncertainty associated with the estimate. However, the true uncertainty range cannot be estimated. One major problem with the confidence ranges is the implicitly assumed stationarity of the PDFs of rainfall and of the covariability between predictands and predictors. Under global warming it is likely that the statistical properties will change. The general assumption is that precipitation on a global scale will shift toward more extreme events on the one side and more severe droughts on the other side (Held and Soden 2006). Whether rain over Hawaii will follow this general scenario is not known yet, but it is our contention that higher SSTs will lead to higher amounts of precipitable water and thus increases the likelihood of extreme events. Therefore, it remains a major challenge for SD methods to incorporate this type of uncertainty into the confidence range. Dynamical downscaling methods with regional climate models are ideal tools to take these aspects into account (Schmidli et al. 2007), but the extremely high computational costs of such models will require a well-justified selection of the atmospheric boundary conditions.

For the twenty-first-century climate change projection purpose, the intermodel comparison revealed that the basic dynamic features of the circulation changes vary drastically among the models. The objective quality assessment of the models could not narrow down the ensemble spread. The difficulties of estimating the rainfall changes in the area around Hawaii were already present in the IPPC report (Fig. 11.25 in Solomon et al. 2007). Part of the spread in the model ensemble is the result of different dynamical responses over the Pacific region (Barsugli et al. 2006; Solomon et al. 2007; Vecchi et al. 2008). In fact, this region is under the direct control of the atmospheric response to ENSO and the PDO (Chu 1995; Chu and Chen 2005). ENSO's response to increased twenty-first-century CO_2 levels is not well defined in the ensemble, and differences in the atmospheric teleconnection pattern result in ambiguous circulation response pattern. Therefore, it is not surprising that the region around Hawaii exhibits low coherency in the climate change scenarios among the models. In this context, it must also be mentioned that the global scaling arguments of Held and Soden (2006) (see also Vecchi et al. 2006; Mitas and Clement 2005) cannot immediately be projected onto the regional scales of Hawaii. As discussed in Held and Soden (2006), the trade winds are expected to weaken on a zonal average, but for Hawaii the changes in the stationary eddies (i.e., the subtropical cell) are of crucial importance (Barsugli et al. 2006). The application of the theory and the statistical results presented here for the AR4 scenarios are not contradicting each other.

The uncertainty inherent in the ensemble of the GCM models is directly passed through the statistical transfer model onto the estimated station rainfall anomalies. The transfer function cannot reduce this type of climate change uncertainty. Neither can regional models overcome this uncertainty. Future generations of GCMs are expected to provide more consistent circulation scenarios over the Pacific. Finally, the emission scenarios themselves are highly disputed. In addition to the statistical uncertainties and the model differences, the wide range of

likely emission scenarios also adds a significant amount of uncertainty to the Hawaiian rainfall change scenarios.

Based on the IPCC AR4 A1B scenarios we find that the potential exists for the Hawaiian Islands to experience significant changes in the circulation pattern. Our SD projects moderate rainfall changes for Hawaii by the end of the twenty-first century as a consequence of the circulation changes. In one of the six analyzed model scenarios, an increase of 20%–30% in the wintertime rainfall is projected. Taking all six models together, the most likely projection is a 5%–10% decrease during the wet winter season by the end of the twenty-first century. For the dry season the maximum likelihood value has a rather broad distribution. A modest (5%) shift to increased rainfall is indicated. We notice that this study only investigated the mean seasonal rainfall changes and not the extreme events. The results from this SD method are collected online at http://apdrc.soest.hawaii.edu/projects/index.html, and future results with optimized predictors and other climate change scenarios will be added to the Web pages.

Acknowledgments. The authors are grateful to the anonymous reviewers for their constructive criticism. H. F. Diaz was supported by NOAA and the U.S. Department of Energy. O. Timm has been supported by the Japan Agency for Marine-Earth Science and Technology (JAMSTAC) through its sponsorship of the International Pacific Research Center. We thank K. Hamilton for his support and encouragement in this work and L. Mehrhoff from the USGS Pacific Island Ecosystems Research Center, Honolulu, for his support of this project. We are grateful to Thomas Giambelluca for the stimulating discussions.

REFERENCES

Barsugli, J. J., S.-I. Shin, and P. D. Sardeshmukh, 2006: Sensitivity of global warming to the pattern of tropical ocean warming. *Climate Dyn.,* **27,** 483–492, doi:10.1007/s00382-006-0143-7.

Cao, G., T. W. Giambelluca, D. E. Stevens, and T. A. Schroeder, 2007: Inversion variability in the Hawaiian trade wind regime. *J. Climate,* **20,** 1145–1160.

Christensen, J., and Coauthors, 2007: Regional climate projections. *Climate Change 2007*: *The Physical Science Basis,* S. Solomon et al., Eds., Cambridge University Press, 849–926.

Chu, P.-S., 1995: Hawaii rainfall anomalies and El Niño. *J. Climate,* **8,** 1697–1703.

——, and H. Chen, 2005: Interannual and interdecadal rainfall variations in the Hawaiian Islands. *J. Climate,* **18,** 4796–4813.

——, A. J. Nash, and F.-Y. Porter, 1993: Diagnostic studies of two contrasting rainfall episodes in Hawaii: Dry 1981 and wet 1982. *J. Climate,* **6,** 1457–1462.

Gedalof, Z., and D. Smith, 2001: Interdecadal climate variability and regime-scale shifts in Pacific North America. *Geophys. Res. Lett.,* **28,** 1515–1518.

Giambelluca, T., M. Nullet, and T. Schroeder, 1986: Rainfall atlas of Hawaii. Hawai'i Division of Water and Land Development, Tech. Rep. R76, 267 pp.

Held, I. M., and B. J. Soden, 2006: Robust responses of the hydrological cycle to global warming. *J. Climate,* **19,** 5686–5699.

Kang, H., K. An, C. Park, A. L. Solis, and K. Stitthichivapak, 2007: Multimodel output statistical downscaling prediction of precipitation in the Philippines and Thailand. *Geophys. Res. Lett.,* **34,** L15710, doi:10.1029/2007GL030730.

Loope, L. L., 1995: Climate change and island biological diversity. *Islands: Biological Diversity and Ecosystem Function on Islands,* P. M. Vitousek, L. L. Loope, and H. Adsersen, Eds., Springer, 123–131.

——, and T. W. Giambelluca, 1998: Vulnerability of island tropical montane cloud forests to climate change, with specific reference to East Maui, Hawaii. *Climatic Change,* **39,** 503–517.

Lyons, S. W., 1982: Empirical orthogonal function analysis of Hawaiian rainfall. *J. Appl. Meteor.,* **21,** 1713–1729.

Meehl, G., A. Hu, and B. Santer, 2009: The mid-1970s climate shift in the Pacific and the relative roles of forced versus inherent decadal variability. *J. Climate,* **22,** 780–792.

Michaelsen, J., 1987: Cross-validation in statistical climate forecast models. *J. Appl. Meteor.,* **26,** 1589–1600.

Miller, A., D. Cayan, T. Barnett, N. Graham, and J. Oberhuber, 1994: The 1976–1977 climate shift of the Pacific Ocean. *Oceanography,* **7,** 21–26.

Mitas, C. M., and A. Clement, 2005: Has the Hadley cell been strengthening in recent decades? *Geophys. Res. Lett.,* **32,** L03809, doi:10.1029/2004GL021765.

North, G., T. Bell, R. Cahalan, and F. Moeng, 1982: Sampling errors in the estimation of empirical orthogonal functions. *Mon. Wea. Rev.,* **110,** 699–706.

Oki, D. S., 2004: Trends in streamflow characteristics at long-term gaging stations, Hawaii. U.S. Geological Survey, Scientific Investigations Rep. 2004—5080, 124 pp.

Ramage, C. S., and T. A. Schroeder, 1999: Trade wind rainfall atop Mount Waialeale, Kauai. *Mon. Wea. Rev.,* **127,** 2217–2226.

Sanderson, M., 1993: *Prevailing Trade Winds: Weather and Climate in Hawaii.* University of Hawai'i Press, 126 pp.

Schmidli, J., C. M. Goodess, C. Frei, M. R. Haylock, Y. Hundecha, J. Ribalaygua, and T. Schmith, 2007: Statistical and dynamical downscaling of precipitation: An evaluation and comparison of scenarios for the European Alps. *J. Geophys. Res.,* **112,** D04105, doi:10.1029/2005JD007026.

Schroeder, T. A., 1993: Climate controls. *Prevailing Trade Winds: Weather and Climate in Hawai'i,* M. Sanderson, Ed., University of Hawai'i Press, 12–36.

Solomon, S., and Coauthors, 2007: *Climate Change 2007*: *The Physical Science Basis*. Cambridge University Press, 996 pp.

Taylor, K. E., 2001: Summarizing multiple aspects of model performance in a single diagram. *J. Geophys. Res.,* **106** (D7), 7183–7192.

Trenberth, K., 1990: Recent observed interdecadal climate changes in the Northern Hemisphere. *Bull. Amer. Meteor. Soc.,* **71,** 988–993.

Uppala, S. M., and Coauthors, 2005: The ERA-40 Re-Analysis. *Quart. J. Roy. Meteor. Soc.,* **131,** 2961–3012, doi:10.1256/qj.04.176.

Vecchi, G. A., B. J. Soden, A. T. Wittenberg, I. M. Held, A. Leetmaa, and M. J. Harrison, 2006: Weakening of tropical Pacific atmospheric circulation due to anthropogenic forcing. *Nature,* **441,** 73–76, doi:10.1038/nature04744.

——, A. Clement, and B. J. Soden, 2008: Examining the tropical Pacific's response to global warming. *Eos, Trans. Amer. Geophys. Union,* **89,** doi:10.1029/2008EO0900002.

von Storch, H., and F. Zwiers, 1999: *Statistical Analysis in Climate Research*. Cambridge University Press, 484 pp.

——, E. Zorita, and U. Cubasch, 1993: Downscaling of global climate change estimates to regional scales: An application to Iberian rainfall in wintertime. *J. Climate,* **6,** 1161–1171.

Wang, J., and X. Zhang, 2008: Downscaling and projection of winter extreme daily precipitation over North America. *J. Climate,* **21,** 923–937.

Wilby, R., and T. Wigley, 1997: Downscaling general circulation model output: A review of methods and limitations. *Prog. Phys. Geogr.,* **21,** 530–548, doi:10.1177/030913339702100403.

Woodcock, A. H., 1975: Anomalous orographic rains of Hawaii. *Mon. Wea. Rev.,* **103,** 334–343.

Yang, Y., and Y.-L. Chen, 2003: Circulation and rainfall on the lee side of the island of Hawaii during HaRP. *Mon. Wea. Rev.,* **131,** 2525–2542.